Thermal Flux through a Surface of *n*-Octane. A Non-equilibrium Molecular Dynamics Study

Jean-Marc Simon,*,† Signe Kjelstrup,‡ Dick Bedeaux,‡,§ and Bjørn Hafskjold‡

Laboratoire de Recherches sur la Reactivite des Solides, UMR 5613 du CNRS, Universite de Bourgogne, BP 47870, 21078 Dijon Cedex, France, Department of Chemistry, Norwegian University of Science and Technology, NO-7491 Trondheim, Norway, and Leiden Institute of Chemistry, PO Box 9502, 2300 RA Leiden University, Leiden, The Netherlands

We show using non-equilibrium molecular dynamics that there is local equilibrium in the surface when a two-phase fluid of *n*-octane is exposed to a large temperature gradient (10^8 K/m). The surface is defined according to Gibbs, and the transport across the surface is described with non-equilibrium thermodynamics. The structure of the surface in the presence of the gradient is the same as if the interface was in equilibrium, as measured by the variation across the surface of the pressure component that is parallel to the surface. The surface is in local equilibrium by this criterion and because the equation of state for the surface was unaltered by a large heat flux. The surface has a small entropy and is thus more structured than a surface of argon particles. The excess thermal resistance coefficient and the coupling coefficient for transport of heat and mass were calculated and found to be smaller than corresponding coefficients from kinetic theory and for argon-like particles, probably because molecular vibrations contribute to heat transfer. Away from the triple point, the heat of transfer was more than 30% of the value of the enthalpy of evaporation, which means that the surface has a large impact on the heat flux across it. This will be of practical importance in non-equilibrium models for phase transitions. The results support the basic assumptions in non-equilibrium thermodynamics and enable us to give linear flux force relations of transport with surface tension dependent transfer coefficients.

1. Introduction

The region between two phases, the surface, has physical properties that are different from those of the homogeneous phases. The thermodynamic description of the surface in terms of excess variables was worked out already by Gibbs.[1] The excess variables of the surface between a vapor and a liquid are the excess density, entropy, and energy. On a microscopic scale, the surface has a thickness ranging from a few molecular diameters (at the triple point) to infinity (at the critical point of the fluid). On the thermodynamic scale, the surface thickness is integrated out.

While methods and techniques for calculations of equilibrium properties of a surface are well established; such methods are hardly available for a surface in a system that is not in equilibrium. The major aim of this paper is to contribute to the establishment of such methods. Questions of fundamental importance, that shall be addressed in the paper, are: Can we define a surface in the absence of global equilibrium in the system? Can we define local thermodynamic properties also in the case that there are large gradients across it? How can we define the transport properties of the surface? Of course, we are also interested in the values of the transport coefficients.

A first effort to answer these questions was made by Røsjorde et al.[2] using non-equilibrium molecular dynamic simulations (NEMD). The authors studied the liquid–vapor interface in a simple fluid of Lennard-Jones spline particles exposed to large temperature gradients and to pressures that differed from the saturation pressure. An important finding was that the surface tension at global equilibrium in the system was the same as the surface tension in a temperature gradient, for the same surface temperature. The surface temperature was defined using the kinetic energy of the interface layer. In other words, the surface was in local equilibrium. The hypothesis of local equilibrium is central to non-equilibrium thermodynamics. Once it is valid, we can use this theory to set up transport equations for the system. Heat and mass transfer coefficients were found for the argon-like particles, specific for the surface. Near the triple point they compared well with results from kinetic theory. However, the coefficients did not agree with experimental results reported by Fang and Ward.[3,4] These authors measured large temperature jumps at an evaporating surface of water, octane, and methyl-cyclohexane. These temperature jumps were an order of magnitude larger than those predicted by kinetic theory and NEMD. The molecular structure may be important in this respect. It has been proposed that the rotational degree of freedom in the molecule determines its probability of condensation. An important aim of this article is thus to see if vibrational and rotational degrees of freedom in the molecule alter the conclusions above or account for the discrepancy between non-equilibrium molecular dynamics simulations and experiments.

This gives the background for choosing *n*-octane as a case study. The same molecule was used in the experiments of Ward et al.[3,4] Transport properties for the liquid and vapor phases of linear *n*-alkanes are known from experiments as well as from simulations.[5–10]

NEMD is an excellent tool to study the questions raised above. It can be used to find transport properties as well as to

---

* Corresponding author. E-mail: jmsimon@u-bourgogne.fr
† Universite de Bourgogne.
‡ Norwegian University of Science and Technology.
§ Leiden University.

Thermal Flux through a Surface of *n*-Octane

J. Phys. Chem. B, Vol. 108, No. 22, 2004 **7187**

create two-phase systems with an explicit stable surface. Equilibrium molecular dynamics (EMD) simulations give equilibrium properties for the system. Equilibrium properties can also be generated by the Gibbs ensemble Monte Carlo (GEMC) method,[11−13] but this method is not suitable for our purpose because it does not model the surface. A further advantage of NEMD is the possibility to gain understanding of the mechanisms involved.

The paper is structured as follows. We give the entropy production rate that governs the transport processes in section 2. The model for *n*-octane is described in section 3. In section 4, we describe how we compute equilibrium properties and transport properties of the system. The resulting equilibrium properties are presented in section 5, followed by the transport properties. The properties of the system out of equilibrium are then discussed with reference to the equilibrium properties in section 6.

We shall see that the surface indeed can be described by its equation of state, even if the total system is subject to a temperature gradient larger than 10^8 K/m. The predicted behavior of the excess entropy production rate is next confirmed. We establish some, but not all, transfer coefficients. Their values are found to be smaller than predicted by kinetic theory. They are also orders of magnitude smaller than calculated from the experimental results. We demonstrate that the structure of the surface stays unaltered in the high-temperature gradients.

2. Non-equilibrium Thermodynamic Theory

The excess entropy production rate of the surface, σ^s, contains the relevant thermodynamic information about the non-equilibrium properties of the system. In the stationary state, we have for transport of heat and mass:[18]

$$\sigma^s = J_q'^l \left(\frac{1}{T^l} - \frac{1}{T^s} \right) + J_q'^g \left(\frac{1}{T^s} - \frac{1}{T^g} \right) - J\frac{1}{T^s}(\mu^l(T^s) - \mu^g(T^s)) \tag{1}$$

Positive transport is defined as being from the vapor to the liquid. There is a heat flux into the surface from the gas, $J_q'^g$, and a heat flux out of the surface into the liquid, $J_q'^l$. The surface has a separate temperature T^s (the surface can accumulate heat). The temperature next to the surface on the liquid side is T^l, and on the gas side it is T^g. The driving force that is conjugate to the mass flux, J, is the chemical potential difference between the two sides of the surface over the temperature. The notation follows de Groot and Mazur.[14] The energy flux through the surface is constant in stationary state:

$$J_e = J_q'^l + h^l J = J_q'^g + h^g J \tag{2}$$

With $\Delta_{vap}H = h^g - h^l$ we have

$$J_q'^l = J_q'^g + J\Delta_{vap}H \tag{3}$$

This relation can be used to eliminate the term containing $J_q'^l$ in the entropy production rate. By using the identity $\mu = h - Ts$, we obtain

$$\sigma^s = J_q'^g \left(\frac{1}{T^l} - \frac{1}{T^g} \right) + J\frac{1}{T^l}[\mu^g(T^g) - \mu^l(T^l) - s^g(T^g - T^l)]$$

By expanding the chemical potentials around the temperature they refer to, and taking the entropy of the gas constant in the

temperature interval (a good assumption), we obtain

$$\sigma^s = J_q'^g \left(\frac{1}{T^l} - \frac{1}{T^g} \right) - J\frac{1}{T^l}[\mu^l(T^l) - \mu^g(T^l)]$$

The chemical potential of the gas at the liquid temperature is

$$\mu^g(T^l) = \mu^{g,o}(T^l) + RT^l \ln\frac{f^g}{f^o} \tag{4}$$

where f^g is the fugacity of the gas, R is the gas constant, and superscript o denotes the standard state. The vapor is frequently nonideal for conditions leading to condensation. This is, for instance, the case here. The chemical potential of the pure liquid can be expressed by the chemical potential of a vapor in equilibrium with the liquid at its temperature, T^l. This gives

$$\mu^l(T^l) = \mu^{g,o}(T^l) + RT^l \ln\frac{f^*}{f^o} \tag{5}$$

where f^* is the fugacity of the saturated vapor. The entropy production rate defines the two independent forces and fluxes of transport for the surface:

$$\Delta\left(\frac{1}{T}\right) = r_{qq}^s J_q'^g + r_{q\mu}^s J = -\frac{\Delta T}{T^g T^l} \tag{6}$$

$$-R \ln\frac{f^g}{f^*} = r_{\mu q}^s J_q'^g + r_{\mu\mu}^s J \tag{7}$$

Here $\Delta(1/T) = (1/T^l) - (1/T^g)$, and J is positive for a condensing vapor. The forces depend on the fluxes through the phenomenological coefficients r_{ij}^s. There are two main coefficients, for heat transfer and for mass transfer, r_{qq}^s and $r_{\mu\mu}^s$, respectively. The coupling coefficient $r_{q\mu}^s$ describes the resistance to transport of mass across the phase boundary, while $r_{\mu q}^s$ is the resistance to heat transfer from the gas phase ($J_q'^g$). The two coefficients are equal, $r_{q\mu}^s = r_{\mu q}^s$.[15,16] The coefficients were given in terms of kinetic theory.[17,18] We study here heat transport in the absence of mass transport. A temperature jump is produced across the surface. It follows from eq 6 that

$$\Delta T = - T^g T^l r_{qq}^s J_q'^g \tag{8}$$

The heat of transfer is defined by

$$q^{*,s} = \left(\frac{J_q'^g}{J} \right)_{\Delta T=0} = \frac{r_{q\mu}^s}{r_{qq}^s} \tag{9}$$

We shall here find the heat of transfer, using the Onsager relation $r_{q\mu}^s = r_{\mu q}^s$ and

$$q^{*,s} = \frac{r_{\mu q}^s}{r_{qq}^s} = \left[\frac{-R \ln f^g/f^*}{\Delta(1/T)} \right]_{J=0} \tag{10}$$

We shall find the coefficients r_{qq}^s, $r_{\mu q}^s$, and thus $q^{*,s}$ for a surface of *n*-octane in this investigation.

3. The System

3.1. System Boundaries. The system, or the MD cell, contained $N_{mol} = 2000$ molecules and had a fixed volume, V. The cell was rectangular, with length ratios $L_x/L_y = L_x/L_z = 8$, where L_i was the length of the cell in the ith direction. In the *x*-direction, the cell was artificially divided into 400 equal subvolumes, called layers, to improve the analysis, see Figure
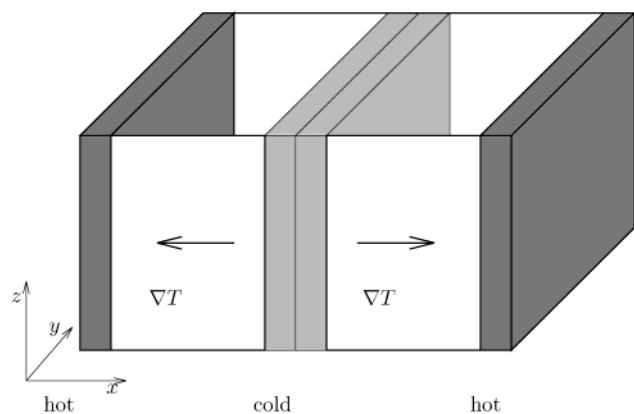
Figure 1. NEMD cell.

1. The position of a molecule in the cell was given by its center of mass. A molecule belonged to a layer if its position was located in that layer. The 10 layers at the ends of the cell were defined as hot zones, and the 20 central layers as a cold zone, see Figure 1. The temperatures in these layers were T_h and T_{co}, respectively, with $T_{co} < T_h$.

A temperature gradient was created across the box in the x direction by modifying the temperature of the molecules in the *cold* and *hot* zones. To fix T_{co} or T_h, the kinetic energy of all molecules in the zone was modified appropriately, in each time step in the calculation. The momentum was conserved during the operation. On the average, kinetic energy was added to the hot zone, and removed from the cold zone. An internal energy flux was then created, specific for the temperature gradient.

The box was replicated in the directions perpendicular to the heat flux to give periodic boundary conditions (PBC) in three dimensions. The system therefore developed two temperature gradients and two internal energy fluxes. Because of PBC, these fluxes and gradients had the same magnitude but were opposite in sign. System properties were computed for each layer and the average was taken of symmetric layers (computational details are given below).

By choosing the proper overall mass density, ρ, and temperatures from the phase diagram, the temperature gradient generated a liquid region in the center of the cell, and vapor on both sides. It was important to choose the overall mass density also such that the vapor region was much thicker than the mean free path. To address the question whether one is in the vapor or "in the surface", it is crucial to have such a sufficiently thick vapor layer. The overall mass density of the system was chosen to be 167.5 kg/m³, which is a value that resulted in a phase separation with proper boundary conditions.

The size of the cell was $V = L_x L_y L_z = 2000\ M/N_A \rho$ where N_A is Avogadro's number, and M the molar mass. The length of the cell in the x direction, L_x, and the layer thickness, then became 524.95 and 1.31 Å, respectively. The mean free path was calculated using the standard formula, $l = M/(r_0^2 \rho \pi N_A \sqrt{2})$, from kinetic gas theory where r_0 is the diameter of the particles. For n-octane, we choose r_0 to be the sum of two mean distances between two adjacent carbons d_{cc} plus the value of the Lennard-Jones parameter σ for the methylene cf. Table 1. This gave $r_0 = 6.6$ Å.

3.2. Model of n-Octane and Molecular Interaction Potential. We used the anisotropic united atoms (AUA) model proposed by Toxvaerd[19] to model n-octane. In that model n-octane is a chain of eight connected united atoms or pseudoatoms. The methyl (CH$_3$) and methylene (CH$_2$) groups are considered as one united atom (UA) each, or one center of

TABLE 1: Model and Potential Data[5]

bond length and AUA distances:		
$d_{cc} = 1.54$ Å	$d_1 = 0.275$ Å	$d_2 = 0.370$ Å
mass of the interacting sites (kg·mol^{-1}):		
$m_{CH_2} = 0.014$	$m_{CH_3} = 0.015$	
Lennard-Jones potential:		
CH$_2$	$\epsilon/R = 80$ K	$\sigma = 3.527$ Å
CH$_3$	$\epsilon/R = 120$ K	$\sigma = 3.527$ Å
bending potential:		
$\beta_0 = 114.6°$	$k_\beta = 520$ kJ mol^{-1}	
torsion potential /kJ mol^{-1}:		
$a_0 = 8.6279$	$a_1 = 20.170$	$a_2 = 0.67875$
$a_3 = -26.018$	$a_4 = -1.3575$	$a_5 = -2.1012$

force. In the AUA model, the positions of the interaction sites are shifted from the center of mass of the carbon atoms to the geometrical center of the methyl (CH$_2$) and methylene (CH$_3$) groups.[5] In this way, the site−site interactions depend on the relative orientations of the interacting chains, as in real molecules. The magnitude of the shift is noted d_1 for CH$_2$ and d_2 for CH$_3$. This model gave simulation results for the diffusion coefficient, the pressure, and the trans-gauche configuration in excellent agreement with experimental data for n-pentane and n-decane in the liquid phase.[5] All potential parameters can be found in Table 1.

The site−site intermolecular interaction was a truncated Lennard-Jones potential:

$$V_{LJ}(r_{ij}) = \begin{bmatrix} 4\epsilon_{ij}\left[\left(\dfrac{\sigma_{ij}}{r_{ij}}\right)^{12} - \left(\dfrac{\sigma_{ij}}{r_{ij}}\right)^6\right], & r_{ij} < r_c \\ 0, & r_{ij} \geq r_c \end{bmatrix} \quad (11)$$

where r_c is the potential cut-off radius, r_{ij} is the distance between sites i and j, and σ_{ij} and ϵ_{ij} are the potential parameters. We used the Lorentz−Berthelot mixing rules $\epsilon_{ij} = (\epsilon_{ii}\epsilon_{jj})^{1/2}$ and $\sigma_{ij} = (\sigma_{ii} + \sigma_{jj})/2$ where ϵ_{ii} and σ_{ii} are the potential parameters for like site interactions.

In addition to the intermolecular site−site interactions, the atomic units (CH$_2$ and CH$_3$) are affected by intramolecular constraints and forces. The carbon−carbon bond lengths d_{cc} are constrained to their mean value using the RATTLE algorithm by Andersen.[20] The angle bending potential was

$$V_B(\beta) = \frac{1}{2}k_\beta(\cos\beta - \cos\beta_0)^2 \quad (12)$$

where k_β is the bending force constant, β_0 is the equilibrium bond angle, and β is the instantaneous bond angle. The torsion potential was a fifth-order polynomial in $\cos\phi$, where ϕ is the dihedral angle:

$$V_T(\phi) = \sum_{i=0}^{5} a_i(\cos\phi)^i \quad (13)$$

The intramolecular potential also includes Lennard-Jones interactions between sites separated by three or more centers. The site−site cutoff radius r_c was 2.5 σ_{LJ}. We have used a neighbor list with a site−site list radius, $r_l = 1.1\ r_c$. Several authors[22,23] underlined the importance of the length of the cutoff radius on the results, the shape of the coexistence curve, and the surface tension. The cutoff radius used here was necessary to obtain acceptable computational times. The values adopted for the interaction potential are given in Table 1.

4. Calculations

4.1. Solution Procedure. The basis of NEMD simulations is described elsewhere.[24,25] We shall describe only some relevant details.

TABLE 2: Simulation Conditions

sim. no:	T/K eq.	T_{co}/K	T_h/K
1	293		
2	321		
3	335		
4	355		
5	380		
6		320	420
7		320	500
8		350	450
9		350	500
10		350	550

The equations of motion were solved using the *Verlet* velocity algorithm[26] with a time-step of 0.005 ps. In all cases, we started with a homogeneous distribution of matter and with a Maxwellian distribution of velocities in all layers. Each distribution was defined by setting the temperature. After a period of equilibration, the temperatures in layers 1−10 and 390−400 were changed to temperatures slightly higher than the equilibrium value. In layers 190−210, the temperature was then reduced by a few Kelvin. In this way, a preliminary stable surface was first established in 50 ps. In subsequent EMD simulations (obtained after switching off the NEMD procedure), the temperature and density stabilized in 200 ps (40 000 time steps). The NEMD simulations started with a transient period, the time for the gradient of temperature and density to be stable. This period lasted 400 000 time steps and it was discarded, since we were interested in the stationary state.

The fluxes and variables in all 400 layers of the system were found as time averages of instantaneous velocities, kinetic energies, potential energies, and the number of particles. Potential energies were calculated using the unshifted cutoff potentials. Using the symmetry of the system around the middle of the box, the mean of the properties in each half was calculated to obtain better statistics. This gives a system with only 200 layers, where each layer is the mean of the corresponding two layers in the original system. To obtain small uncertainties, for both EMD and NEMD simulations, analysis runs were carried out for 3.2 ns (640 000 time steps). The 2000 molecules contained altogether $N_{at} = 16\,000$ centers of force or atoms, and each run required about 2 weeks on a XP1000 Dec workstation. Under these conditions, the statistical uncertainty for each layer in the computed density was less than 3% (3% in the vapor phase and 0.3% in the liquid phase), and in the temperature was less than 0.5%.

4.2. Cases Studied. Ten simulations were run for the two-phase fluid system. Five simulations were done for equilibrium conditions, and five under non-equilibrium conditions. In the last cases, variations in density, temperature, and pressure were computed across the cell. In addition, the heat flux was calculated. The temperature gradients in the study exceed normal laboratory values by several orders of magnitude. They were of the order of 10^9 K/m in the vapor and 10^8 K/m in the liquid. The surface was thus investigated in the absence and presence of a heat flux. Table 2 contains the characteristics of these 10 simulations.

4.3. Molar Density Calculation. The molar density of the layers $\rho_{m\nu}$ was given by the number of molecules, N_ν, in each pair of layers divided by the volume of the pair of layers ν and Avogadro's number:

$$\rho_{m\nu} \equiv N_\nu \frac{200}{VN_A} \qquad (14)$$

The mass density ρ_ν was simply calculated as the product of $\rho_{m\nu}$ by the molar mass of the octane.

4.4. Temperature Calculation. In each pair of layers ν, the kinetic temperature, T_ν, was given by the different definition of the kinetic energy K_ν

$$K_\nu = \frac{1}{2}N_\nu n_{df}kT_\nu = \frac{1}{2}\sum_{\alpha=1}^{N_\nu}\sum_{i=1}^{8}m_i|\mathbf{v}_{i\alpha} - \mathbf{v}_\nu|^2 \qquad (15)$$

where $\mathbf{v}_{i\alpha}$ was the instantaneous velocity of the united atom i of the molecule α and $\mathbf{v}_\nu$ was the barycentric instantaneous velocity of the layer ν. The term n_{df} is the number of degrees of freedom per molecule of *n*-octane; here $n_{df} = 17$. For convenience in the following we will use Latin letters to identify the united atoms and Greek letters to identify the molecules. By using the assumption of equipartition, one may identify the temperature of the layer with the kinetic temperature.

The surface temperature, T^s, was calculated by assuming that the previous equation was valid for the whole surface area, not only for a specific layer ν. Under that condition T^s might be seen as the average of the individual kinetic temperatures of all the molecules located in the surface.

4.5. Total Energy Calculation. The total energy of the pair of layers U_ν was the sum of the kinetic energy and the potential energy of the molecules located in the layers. This potential energy included the intramolecular energy and the intermolecular (Lennard-Jones) energy of the molecules interacting with molecules located in the same layer or in other layers. By dividing by N_ν, we obtained the energy per mol, k_ν for the kinetic energy and u_ν the total energy.

4.6. Pressure Components, Surface Tension, and Heat Flux Calculations. Two different methods shall be used to find the components of the pressure normal and parallel to the surface, namely the Irving-Kirkwood method (here called IK1)[27] and the method of planes (MOP) after Todd and Evans.[28] The surface tension shall be found with pressure components from both methods, while the heat flux is calculated using MOP expressions.

Irving and Kirkwoood[27] gave in 1950, the pressure in a fixed volume as a sum of a kinetic (perfect gas) term and a Taylor expansion of the interaction potential around the vector distance between interacting center of forces. In homogeneous systems, the second and higher order terms of the expansion vanish and give the usual expression of the pressure tensor that we have used here, see eq 16, and called IK1. In nonhomogeneous systems, the second order term and higher order terms have a nonzero contribution, due to nonsymmetry of matter at long distances around each center of mass. The calculation of the pressure with the full expression is very time consuming, and thus the IK1 expression is commonly used as a first approximation.

The IK1 pressure tensor was obtained by time averaging the microscopic pressure tensor

$$p_{ab} = \frac{200}{V}\sum_{\alpha\in layers\nu}\left(m_\alpha v_{\alpha,a}v_{\alpha,b} + \sum_{\beta\neq\alpha}F_{\alpha\beta,a}\,r_{\alpha\beta,b}\right)$$
$$(a,b = x, y, z) \quad (16)$$

where $v_{\alpha,a}$ is the velocity of the molecule α in the direction a, and $F_{\alpha\beta,a}$ is the force exerted on molecule α by the molecule β in the direction a. Finally $r_{\alpha\beta,b}$ is the component of the vector from molecule β to molecule α in the direction b.

Todd and Evans[28] derived the same initial full expression as Irving and Kirkwood for planes, instead of for volumes, to study the Poiseuille flow. They obtained the simple expression 17 for the pressure normal to a given plane, for a system being

homogeneous in that plane. They called this expression and the method to get it the "Method Of Planes" (MOP). The MOP expression for the pressure of the plane $A = L_y L_z$ at the position r_x is the sum of a kinetic, p_{xx}^K, and a configurational contribution, p_{xx}^V:

$$p_{xx} = p_{xx}^K + p_{xx}^V \tag{17}$$

where p_{xx}^K is the time average of the momentum flux of the molecules crossing the plane:

$$p_{xx}^K = \frac{1}{A} \sum_{\alpha=1}^{2000} m_\alpha v_{\alpha,x} \, sgn(v_{\alpha,x}) \tag{18}$$

and

$$p_{xx}^V = \frac{1}{4A} \sum_{\alpha=1}^{2000} \sum_{\beta \neq \alpha} F_{\alpha\beta,x} [sgn(r_{\alpha,x} - r_x) - sgn(r_{\beta,x} - r_x)] \tag{19}$$

The pressure tensor is found to be diagonal. Away from the surface the diagonal elements in the x, y, and z directions are the same. In the neighborhood of the surface it is found that the diagonal elements along the surface, $p_\parallel = p_{yy} = p_{zz}$, and normal to the surface, $p_\perp = p_{xx}$, are different. Ikeshoji[29] has later improved the calculation further.

The surface tension was found from the difference between the parallel (IK1) and normal (MOP) components of the pressure, using the expression

$$\gamma = \frac{L_x}{400} \sum_{\nu=1}^{200} (p_\parallel - p_\perp) \tag{20}$$

The expression follows from the usual integral over the surface, taking the pressures constant in each layer. The reason that we divide through 400 rather than 200 is that there are 2 liquid—vapor interfaces in the cell. Otherwise we obtain the sum of the surface tension of both surfaces.

An additional advantage of MOP is that it also gives an expression for the internal energy flux $\mathbf{J}^U$.[30] The very simple expression of the energy flux by MOP, see eq 21, was therefore used here to compute the heat flux which is equal to the energy flux, J_e. The MOP expression of the internal energy flux is a sum of the kinetic, J_{xx}^K, and a configurational part, J_{xx}^V:

$$J_{xx}^U = J_{xx}^K + J_{xx}^V \tag{21}$$

where J_{xx}^K is the time average of the internal energy flux of the molecules crossing the plane:

$$J_{xx}^K = \frac{1}{A} \sum_{\alpha=1}^{2000} u_\alpha sgn(v_{\alpha,x}) \tag{22}$$

where u_α is the internal energy of the molecule α and

$$J_{xx}^V = \frac{1}{4A} \sum_{\alpha=1}^{2000} \sum_{\beta \neq \alpha} \mathbf{v}_\alpha \mathbf{F}_{\alpha\beta} [sgn(r_{\alpha,x} - r_x) - sgn(r_{\beta,x} - r_x)] \tag{23}$$

At stationary state, without mass flux, the conditions of the analysis, we have from equations (2 and 3)

$$J_{xx}^U = J_e = J_q'^l = J_q'^g$$

5. Results

We report first the results for the surface in equilibrium, from simulations number 1−5, and use them to derive thermodynamic
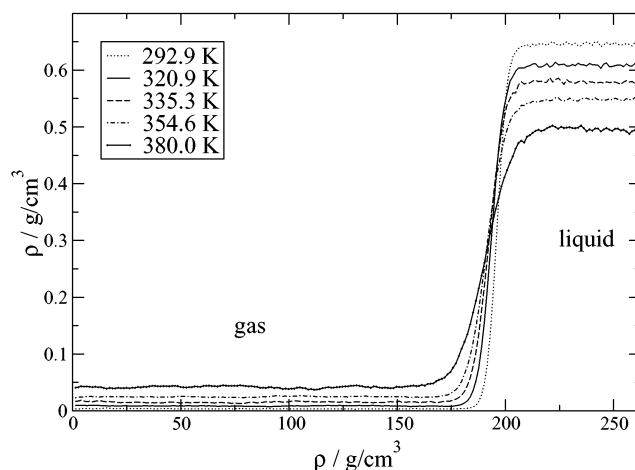

Figure 2. Density profiles at equilibrium for five temperatures (cases 1−5).

properties of the surface. The properties for simulations number 6−10 are next presented. The non-equilibrium simulations fall in two groups. Simulations 6 and 7 refer to the same cold temperature (320 K) and therefore practically the same surface temperature. Simulations 8, 9, and 10 refer to a higher cold temperature (350 K). The results at the higher temperature have a higher scatter.

5.1. Properties of the Surface in Equilibrium. Figure 2 shows the density variation across the box in cases 1 to 5. The density in the liquid phase decreases with the temperature. In the gas phase, the density increases with the temperature. This shifts the relative amount of the two phases in the box as the temperature changes. The thickness of the surface was determined by fitting the density in Figure 2 to the relation

$$\rho(x) = \frac{1}{2}(\rho_L + \rho_V) - \frac{1}{2}(\rho_L - \rho_V) \tanh\left(\frac{x - x_0}{d}\right) \tag{24}$$

Here d is the half thickness of the surface and x_0 is the position of the Gibbs dividing surface:

$$\rho(x_0) = \frac{1}{2}(\rho_L + \rho_V) \tag{25}$$

The extension of the surface was determined as the distance between two positions, where the density was 5% off (or about 2 times the uncertainty in the density) the liquid or vapor density, respectively.

The thicknesses obtained in this manner varied between 3.0 (case 1) and 7.0 nm (case 5). This method of determination did not give significantly different values from the method that we used earlier,[31] where we used deviations from the equation of state for the fluid phases to find the position of the surface.

The critical temperature, T_c, was found by fitting the mass density difference to the equation

$$\rho_L - \rho_V = \rho_0 \left(\frac{T_c - T}{T_c}\right)^\beta \tag{26}$$

with the critical exponent $\beta = 0.32$. The fit is shown in Figure 3. The critical density ρ_c was found by fitting the sum of the coexistence mass density to the law of rectilinear diameters:

$$\frac{\rho_L + \rho_V}{2} = \rho_c + A(T - T_c) \tag{27}$$

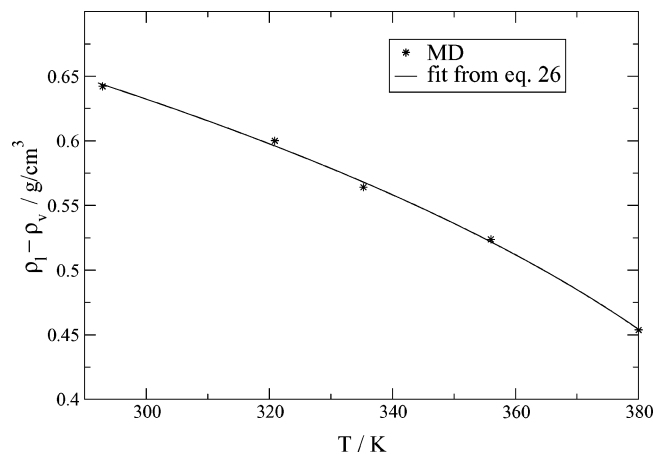This fit is not shown. The fits gave the critical temperature T_c

Figure 3. Density difference plot for determination of the critical temperature (cases 1−5) from eq 26.
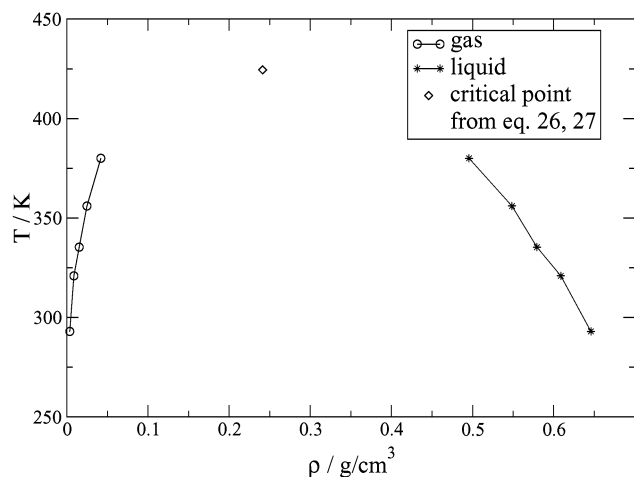

Figure 4. Liquid−vapor coexistence curve from cases 1−5.

= 424.2 K and the density ρ_c = 241.1 kg m^{-3}. The log of the vapor pressure was plotted as a function of the inverse temperature and fitted to the Clausius−Clapeyron equation:

$$p(T) = p^* \exp\left(-\frac{\Delta_{vap}H}{RT}\right) \qquad (28)$$

where p^* is a reference pressure and $\Delta_{vap}H$ is the heat of evaporation per mole. (The plot is not shown.) The equation assumes that $\Delta_{vap}H$ is constant over the range of temperatures that are studied. This assumption is not true, especially close to the critical point where $\Delta_{vap}H$ vanishes. Despite this, all vapor pressures could be fitted to the equation with an accuracy of a few percent. The results were p^* = 49.76 × 10^8 Pa and $\Delta_{vap}H$ = 27.29 kJ/mol. By introducing the critical temperature reported above (424.2 K), we obtained the critical pressure P_c = 22.7 10^5 Pa. The experimental value for *n*-octane is, for comparison, 24.9 × 10^5 Pa.[21]

A Soave−Redlich−Kwong (SRK) equation of state[21] was found for the vapor phase

$$p(T) = \frac{RT}{v_m - b} - \frac{a}{v_m(v_m - b)} \qquad (29)$$

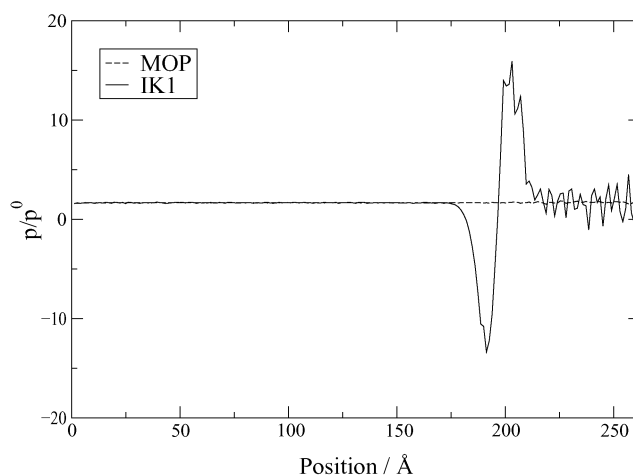where v_m is the molar volume and a and b are coefficients. The

Figure 5. Pressure normal to the surface in case 2 (321 K) calculated with the method of plane (MOP) and the Irving−Kirkwood method (IK1).
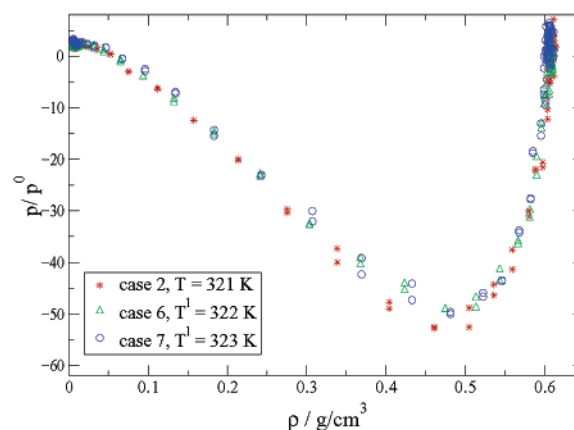

Figure 6. Pressure parallel to the surface as a function of the local density in the surface, in equilibrium (case 2, at 321 K), and out of global equilibrium (cases 6 and 7 with T_{co}= 320 K).

results for *n*-octane were

$$b = \frac{0.08664RT_c}{P_c} \qquad (30)$$

and

$$a(T) = 0.42748\frac{R^2 T_c^2}{P_c}[1 + 0.398(1 - T_r^{1/2})] \qquad (31)$$

where the reduced temperature, $T_r = T/T_c$, has been introduced. The pressures calculated from this equation with the MD critical temperature and pressure agree within 10% with the MD pressures.

The normal and parallel components of the pressure to the surface are shown in Figures 5, 6 and 7 where p^0 = 10^5 Pa is the standard pressure. Consider first the pressure normal to the surface, calculated by the IK1 and the MOP formula. Figure 5 gives the results for case 2 (the variations were the same for all cases 1−10). From the condition of mechanical equilibrium, it follows that the normal component of the pressure is everywhere constant. The pressure components were the same in the bulk phases for both methods, but the methods gave different results in the surface. Only the method of plane gave a constant normal pressure in the surface, but the surface tension from eq 20 was
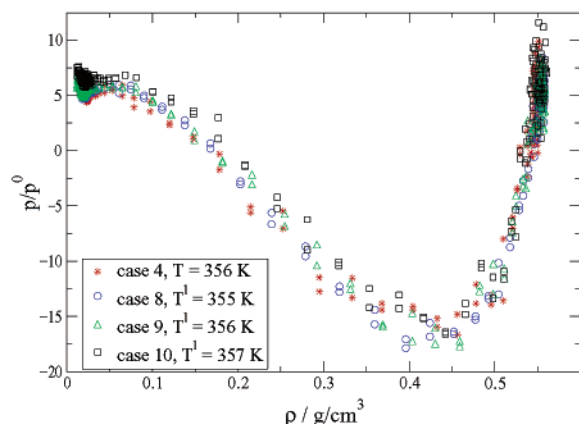
Figure 7. Pressure parallel to the surface as a function of the local density in the surface, in equilibrium (case 4, at 355 K), and out of global equilibrium (cases 8, 9, and 10 with T_{co}= 350 K).
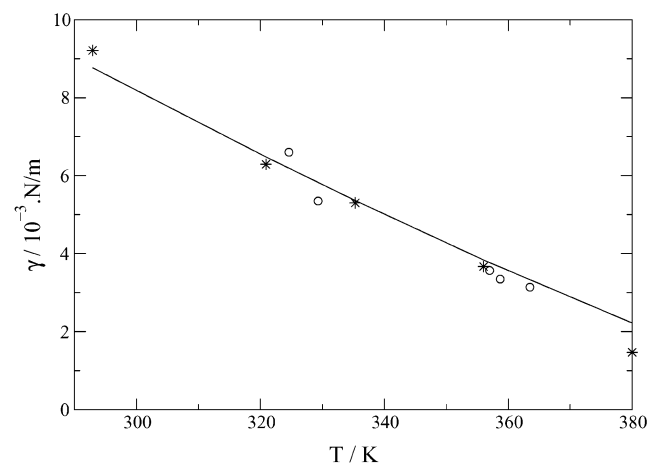

Figure 8. Surface tension as a function of temperature for Cases 1−5 (★) and cases 6−10 (○); the whole line is a fit of the equilibrium data (cases 1−5) from eq 32.

the same with both methods. After this was established, we continued to use the MOP formula.

The component of the pressure that is parallel to the surface is shown for case 2 in Figure 7 and for case 4 in Figure 8. Similar results from the non-equilibrium simulations are also shown in these figures.

The equation of state for the surface of a one-component system is the temperature function of the surface tension:

$$\gamma = \gamma_0\left(\frac{T_c - T}{T_c}\right)^\nu \tag{32}$$

The critical exponent $\nu = 1.26$ is universal. By fitting the results of the equilibrium simulations to this function, we obtained $\gamma_0 = 3.84 \times 10^{-2}$ N/m. The surface tension varied between 9×10^{-3} (case 1) and 2×10^{-3} N/m (case 5).

The entropy density of the surface, s^s, that follows from eq 32 is

$$s^s = s_0\left(\frac{T_c - T}{T_c}\right)^{\nu-1} \tag{33}$$

The results from the simulations gave

$$s_0 = \frac{\nu\gamma_0}{T_c} = 1.14 \times 10^{-4}\text{ J/m}^2\text{K} \tag{34}$$
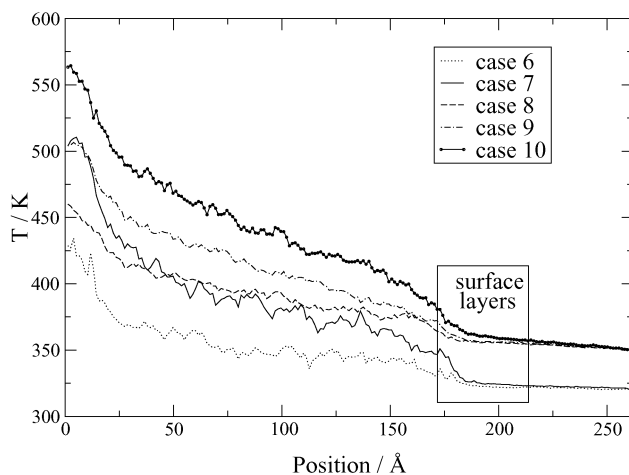

Figure 9. Temperature profiles generated across the cell for cases 6−10. The position of the surface is indicated by the square.
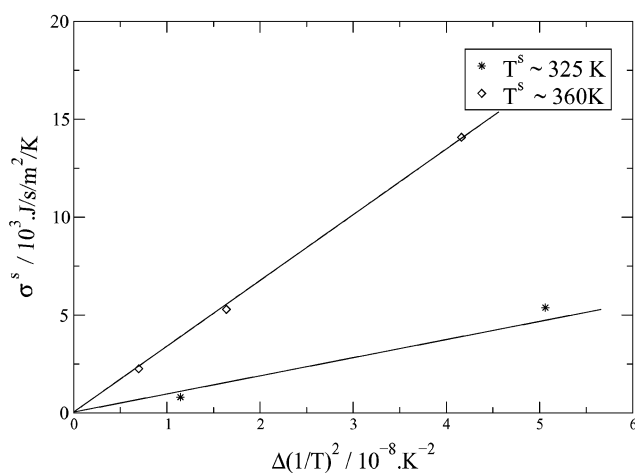

Figure 10. Excess entropy production rate in the surface as a function of the thermal driving force in cases 6, 7 ($T = 320$ K) and cases 8−10 ($T = 350$ K).

The surface entropy density was constant until very close to the critical point where it decreased toward zero.

5.2. Properties of the Surface in a Temperature Gradient. The temperature profiles that were generated in the non-equilibrium simulations, are shown in Figure 9. The temperature decreased monotonically over the box from the gas to liquid (except inside the high temperature zones). The slopes of the curves were approximately constant in the gas and liquid phases, and they were about 10 times higher in the gas than in the liquid. A jump in the temperature was observed at the surface, ranging from 10 to 40 K. The largest part of the jump was close to the gas phase. The surface temperatures were 322 and 323 K for cases 6 and 7, while they were 357, 354, and 355 K, respectively, for cases 8, 9, and 10. (The equilibrium case 2 was for comparison for 321 K, and case 4 was for 355 K.)

The components of the pressure normal and parallel to the surface and the surface tension were calculated also for the cases 6−10 that were out of global equilibrium. The results of these calculations are also shown in Figures 6, 7, and 8. We found that it was not possible to distinguish between the results of cases 1−5 and 6−10, within the accuracy of the calculation.

The excess entropy production rate was next calculated as a function of the driving force. The results are shown in Figure 10. We saw above that the surface temperatures were the same within 1 K in the different sets of experiments. Straight lines
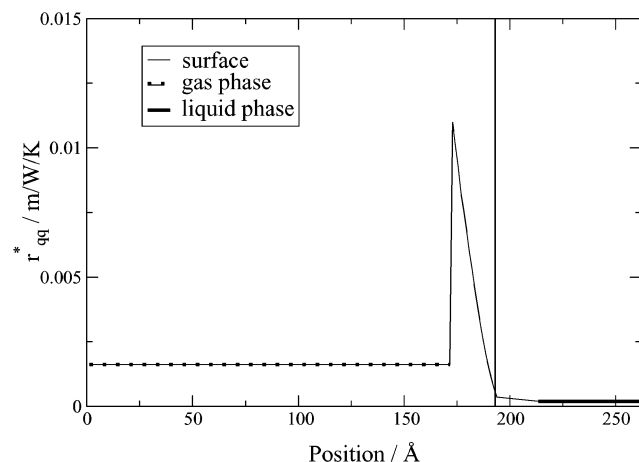
Thermal Flux through a Surface of *n*-Octane

J. Phys. Chem. B, Vol. 108, No. 22, 2004 **7193**

Figure 11. Profile of the thermal resistivity across the surface for state 7. The values of the liquid and gas phases are shown as constants, they are calculated at positions of 100 and 220 Å respectively. The position of the equimolar surface is shown by a vertical line in the figure.

were obtained for each of the two sets, with the curves drawn through origin.

The thermal resistivities of the vapor phase and of the liquid phase were calculated from the gradients of the temperature in the appropriate phases at mean positions of 100 and 220 Å. The local thermal resistivity was also calculated from the gradient of the continuous curve inside the surface. The local thermal resistivity, r_{qq}^*, was everywhere found from

$$\frac{dT}{dx} = - T^2 r_{qq}^* J_q'^g \tag{35}$$

The results are plotted in Figure 11. The figure shows the constant values for the bulk phases and a peak in the surface that is close to the gas side. In that part of the surface, the resistivity is 5 times higher than in the gas phase and 40 times higher than in the liquid phase. The position of the dividing surface, found as described above, is also drawn in the figure. The integral under the curve gave the excess resistivity r_{qq}^s for the surface at temperature T^s. (The dimension of r_{qq}^s is the dimension of r_{qq}^* times *m*.) The result is given below.

The values of r_{qq}^s and $r_{\mu q}^s$ were next found from the simulation results, using eqs 6 and 7 with $J = 0$. The difference in the inverse temperature in eq 6 was taken from the results of Figure 9. The difference in chemical potential at constant temperature in eq 7 was calculated from the vapor pressure (taken from the Soave−Redlich−Kwong equation of state) and from the saturation pressure at T^l (taken from the Clausius−Clapeyron equation, eq 25). The results from eq 8 are plotted as a function of the surface tension on Figure 12. They are also compared with results from kinetic theory in the same figure. For expressions from kinetic theory, see, e.g., Bedeaux and Kjelstrup.[18]

For case 7 we obtained $r_{qq}^s = 8.04 \times 10^{-12}$ m²/W/K from the area under the curve in Figure 11, while the result was 9.4 $\times 10^{-12}$ m²/W/K from the flux equations for this case. The value from the slope of Figure 12, where all points were taken into account, was 9.0×10^{-12} m²/W/K. The coefficients showed in general a larger spread when plotted as functions of the surface tension (Figures 12−14), because a small variation in temperature gave a relatively large variation in surface tension.

The coefficient $r_{\mu q}^s$ and the heat of transfer (the ratio $r_{\mu q}^s/r_{qq}^s$) are shown as a function of the surface tension in Figures 13
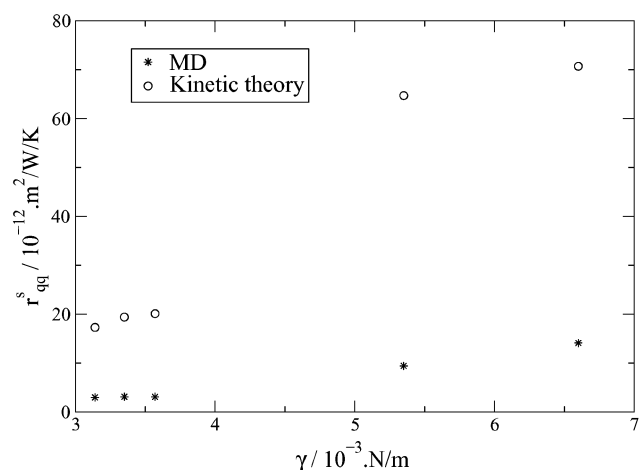

Figure 12. Thermal resistivity of the surface, r_{qq}^s, as a function of the surface tension. The results from kinetic theory are also shown.
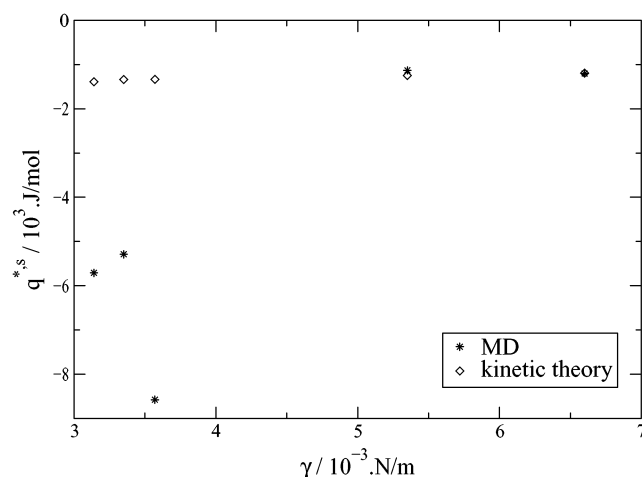

Figure 13. Heat of transfer of the surface, $q^{*,s}$, as a function of surface tension. The results from kinetic theory are also shown.
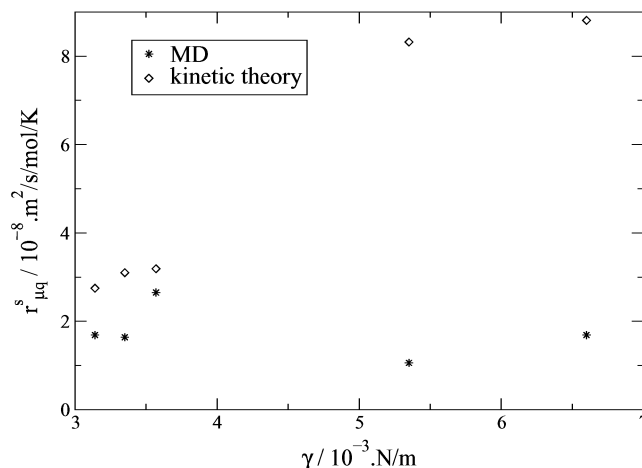

Figure 14. Coefficient $r_{\mu q}^s$ as a function of surface tension. The results from kinetic theory are also shown.

and 14, respectively. They are also compared with values from kinetic theory in the same figures.

6. Discussion

6.1. The Assumption of Local Equilibrium is Valid. The main and surprising finding in this work is that the surface is in local equilibrium, even with the large temperature gradient

that is used in this work. The statement refers to a surface that is defined according to Gibbs. The condition is demonstrated by the equation of state being the same in the absence and presence of temperature gradients. The finding fits well with similar observations for argon-like particles,[31] and for computations with a two-phase van der Waals fluid.[32] The assumption of local equilibrium has here been demonstrated to hold also for a molecular two-phase system.

The assumption of local equilibrium for the surface taken as a whole is a less strong assumption than that of having every part of the surface in local equilibrium.[32] Very surprising is therefore the fact that the plot of the parallel component of the pressure to the surface is the same through the surface, regardless of whether there is a temperature gradient across the system. This was demonstrated by Figure 8 and Figure 9, where this component was plotted as a function of local density through the surface, and compared to the value obtained in global equilibrium. The results from a surface in global equilibrium and from a surface with a temperature gradient are indistinguishable in this figure, within the accuracy of the calculation. This means that the surface maintains its internal structure from the case of global equilibrium, even if a strong temperature gradient is applied to the surface.

6.2. The Entropy Production Rate and the Flux Force Relations. The finding that the assumption of local equilibrium is true gives a strong support for the validity of non-equilibrium thermodynamics. This theory, when applied to surface transport, gives first an expression for the excess entropy production rate, and subsequently the conjugate fluxes and forces of transport. We see that the excess entropy production rate varies with the thermal driving force in a linear way (for almost identical surface temperatures). For a surface temperature near 350 K the line can be extrapolated through zero. The two points for the surface temperature near 320 K, are on a straight line that is drawn through the origin.

This finding means not only that the coefficient of transport is no function of the driving force for a given surface temperature but also that it varies with the surface temperature or the surface tension. This is completely according to what theory predicts. The transport coefficients cannot depend on the driving force; they can, however, depend on the state of the surface. By introducing the condition $J = 0$ into the entropy production rate, we obtain

$$\sigma^s = \left[\Delta\left(\frac{1}{T}\right)\right]^2 / r_{qq}^s(\gamma) \tag{36}$$

In the present case we found the resistance to heat transfer for the high surface temperatures from the above plot. The line with two points only is less certain and was not used.

It follows from the theory that the fluxes are linear in the forces, with surface tension dependent coefficients. Several authors have given equations for evaporation and condensation. According to statistical rate theory, for example, there is a nonlinear relation between the rate of evaporation and its driving force.[3] Nagayama and Tsuruta have recently shown, using MD simulations, that the rate of condensation depends on the particle velocity that is normal to the surface.[33] Their rate of condensation was written using transition state theory. By including the same velocity component as a variable in a mesoscopic level description, Bedeaux et al.[34] showed that the rate expression of Nagayama and Tsuruta could be given a basis in non-equilibrium thermodynamics theory. (Non-equilibrium thermodynamics for the mesoscopic level brings a more detailed mechanistic picture into the thermodynamic description.)

Evidence is thus accumulating, from this work and the works cited above, that linear flux−force relationships are sufficient to describe heat and mass transport across surfaces. Nonlinear flux−force relations are not needed.

6.3. Equilibrium Properties. Equilibrium properties were needed here to calculate the system's driving forces. The properties give also interesting information of the system per se.

We first note that the experimental value of the critical temperature of octane[21] is 25% higher than our value, $T_{c\,exp} =$ 568.8 K. The computed and experimental critical densites agree better, however, within 4%. The difference in critical temperatures can be explained by the short cutoff radius in the potential that is used here, $r_c = 2.5\ \sigma$, see refs 22 and 23. The attractive effect of the dense liquid phase is reduced with this potential, and the critical temperature becomes lower than the real one. Trokhymchuk et al.[22] reported similar results for a Lennard-Jones fluid. Our choice of a cutoff radius was motivated by the necessity to reduce the time necessary to reach stationary state. We do not consider this choice important for the conclusions that are reached about the system's performance.

The enthalpy of evaporation for *n*-octane is more than 5 times larger than the enthalpy of evaporation that we found for argon-like particles.[31] The much higher critical temperature of *n*-octane (424.5 K vs 111.2 K) is thus in accordance with this difference.

It is very interesting to see that the surface entropy is constant with temperature, in the present molecular system. This finding supports an idea of a rather strictly packed layer of *n*-octane at the surface. The surface entropy is small for *n*-octane, $s_0 = 1.14 \times 10^{-4}$ J/m^{2}K, much smaller that the surface entropy of the argon-like particles we studied before, $s_0 = 2.81 \times 10^{-4}$ J/m^{2}K. One would normally expect that a molecule has a higher entropy than an atom, but the surface entropy is a property of the layer, not only the unit in the layer. It will be interesting to see if the small surface entropy of *n*-octane can be linked to a preferred orientation of the long hydrocarbon chain at the surface.

According to common knowledge, $\gamma \approx RT/d^2$, where d is the diameter of the molecule. Argon-like particles should, according to this, have a higher γ_0 than *n*-octane has. This was not found. The value for argon-like particles was 2.48×10^{-2} N/m[31] and the value for *n*-octane was 3.84×10^{-2} N/m. In ref 23, Goujon et al. simulated liquid vapor interfaces of *n*-pentane at equilibrium by MC simulations. They calculated values of surface tensions at different temperatures. From these results and eq 32 we got the values of $\gamma_0 = 6.1 \times 10^{-2}$ N/m $\pm$ 10% N/m, which is higher than for the *n*-octane by a factor 1.6. This gave a ratio of the diameter around 1.3, which qualitatively agrees with the geometry of both molecules.

We conclude that MD simulations give new and interesting knowledge of thermodynamic properties of surfaces.

6.4 Resistivity Coefficients. In this investigation, results from a simulation of a molecular two-phase fluid in a temperature gradient are reported for the first time. We have so far seen that there is no principal difference in behavior of this system and the system of spherical particles that was studied before, Røsjorde et al.[2] The actual values of the thermodynamic and transport properties differ, however. The resistivity coefficients should now be discussed in more detail.

The present investigation allowed for a calculation of two coefficients, r_{qq}^s, and $r_{\mu q}^s$, as functions of surface tension. The coefficient r_{qq}^s was determined in three ways: from the plot of the entropy production rate versus the thermal driving force, from the value of the heat flux and the thermal driving force, and by integrating the excess function r_{qq}^*. The coupling

Thermal Flux through a Surface of *n*-Octane

J. Phys. Chem. B, Vol. 108, No. 22, 2004 **7195**

coefficient was determined from the chemical driving force and the heat flux. It is a good support for the method of analysis that the three different determinations for r_{qq}^s gave the same results.

The values of the thermal resistivity, r_{qq}^s, were around 5 times smaller than those obtained from NEMD simulations with argon-like particles.[2] It is known from studies of bulk phases that the internal structure in the molecule lowers the resistivity to heat transfer.[7] The finding for the surface coefficient, suggests that molecular rotations are active in heat transfer also at the surface. We have earlier found that the larger the surface tension is, the larger is the thermal resistivity. Although *n*-octane, on the average, has a higher surface tension than argon, the variation in the coefficients with surface tension is smaller for *n*-octane. One explanation may be that molecular rotations dampen the effect of a variation in the surface tension on r_{qq}^s.

The cross coefficient $r_{\mu q}^s$ can most easily be explained through the heat of transfer, $q^{*,s}$, the ratio of the two coefficients. The heat of transfer tended to be constant near the triple point. Away from the triple point the value became large, about 30% of the size of the enthalpy of evaporation. For argon-like particles, $q^{*,s}$ became up to 20% of the enthalpy of evaporation.

The values of our coefficients are lower than the values predicted by kinetic theory, also close to the triple point. For the argon-like particles the simulated values were found to agree with kinetic theory values. As kinetic theory does not account for the internal structure of the molecules, the disagreement is not surprising. Kinetic theory also holds for a dilute vapor only. Non-equilibrium molecular dynamics simulations are probably the only way one can have reliable information about surface transport properties away from the triple point.

The effect of the cutoff radius on the coefficients is expected to be important,[35] and should be a subject for further investigation. The results are clearly at variance with experimental results.[3] It is unlikely that we can expect a different order of magnitude by changing the cutoff radius in the interaction potential.

One may ask, since these coefficients are so small, can they then have any impact at all on the performance of the overall system when it is out of global equilibrium? The answer is yes, and it can be attributed to the magnitude of the heat of transfer. This coefficient is large, and influence the heat flux into the vapor considerably. One can thus expect an error in the heat flux by neglecting the contribution from the heat of transfer when there is also mass transfer across the surface. This will be of practical importance.[36]

7. Conclusions

We have shown in this work that the theory of non-equilibrium thermodynamics can be used successfully to describe the behavior of *n*-octane at the interface between liquid and vapor. The underlying assumptions of the theory have been tested and found to apply. The simulation data were reduced to give new information on surface transfer coefficients and surface equilibrium properties.

It is our hope that we, in the future, can offer predictions of surface transfer coefficients when more information will have been collected on the interrelation between the interaction potential, the surface tension, and the transfer coefficients. Two-component systems are interesting targets for future studies, since these are systems of greater technical importance than one-component systems.

References and Notes

(1) Gibbs, J. W. *Collected Works, 2 vols*; Dover: London, 1961.
(2) Røsjorde A.; Kjelstrup, S.; Bedeaux, D.; Hafskjold B. *J. Colloid. Interface Sci.* **2001**, *240*, 355.
(3) Fang, G.; Ward, C. A. *Phys. Rev. E* **1999**, *59*, 417.
(4) Fang, G.; Ward, C. A. *Phys. Rev. E* **1999**, *59*, 441.
(5) Padilla, P.; Toxvaerd, S. *J. Chem. Phys.* **1991**, *94*, 5650.
(6) Simon, J.-M.; Dysthe, D. K.; Fuchs, A. H.; Rousseau, B. *Fluid Phase Equilibria* **1998**, *150−151*, 151.
(7) Simon, J.-M.; Rousseau, B.; Dysthe, D. K.; Hafskjold, B. *Entropie* **1999**, *217*, 29.
(8) Dysthe, D. K.; Fuchs, A. H.; Rousseau, B. *J. Chem. Phys.* **1999**, *110*, 4047.
(9) Dysthe, D. K.; Fuchs, A. H.; Rousseau, B. *J. Chem. Phys.* **1999**, *110*, 4060.
(10) Perronace, A.; Leppla, C.; Leroy, F.; Rousseau, B.; Wiegand, S. *J. Chem. Phys.* **2002**, *116*, 3718.
(11) Panagiotopoulos, A. Z. In *Molecular simulation and industrial applications methods examples and prospects*; Gubbins, K. E., Quirke, N., Eds.; Gordon & Breach: Langhorne, PA, 1996; p 183−205.
(12) Smit, B.; Karaborni, S.; Siepmann, J. L. *J. Chem. Phys.* **1995**, *102*, 2126.
(13) Mackie, A. D.; Tavitian, B.; Boutin, A.; Fuchs, A. H. *Mol. Simul.* **1997**, *19*, 1.
(14) de Groot, S. R.; Mazur, P. *Non-equilibrium thermodynamics*; Dover Publications: New York, 1984.
(15) Onsager, L. *Phys. Rev.* **1931**, *37*, 405.
(16) Onsager, L. *Phys. Rev.* **1931**, *38*, 2265.
(17) Bedeaux, D.; Hermans, L.; Ytrehus, T. *Physica A* **1990**, *169*, 263.
(18) Bedeaux, D.; Kjelstrup, S. *Physica A* **1999**, *270*, 413.
(19) Toxvaerd, S. *J. Chem. Phys.* **1990**, *93*, 4290.
(20) Andersen, H. C. *J. Comput. Phys.* **1983**, *52*, 24.
(21) Prausnitz, J. M.; Lichtenthaler, R. N.; de Azevedo, E. G. *Molecular thermodynamics of fluid-phase equilibria*; Prentice Hall: New York, 1999.
(22) Trokhymchuk, A.; Alejandre, J. *J. Chem. Phys.* **1999**, *111*, 8510.
(23) Goujon, F.; Malfreyt, P.; Boutin, B.; Fuchs, A. H. *J. Chem. Phys.* **2002**, *116*, 8106.
(24) Hafskjold, B.; Ikeshoji, T.; Ratkje, S. K. *Mol. Phys.* **1993**, *80*, 1389.
(25) Hafskjold, B.; Ratkje, S. K. *J. Stat. Phys.* **1995**, *78*, 463.
(26) Allen, M. P.; Tildesley, D. L. *Computer simulation of liquids*; Oxford University Press: Oxford, 1987.
(27) Irving, J. H.; Kirkwood, J. G. *J. Chem. Phys.* **1950**, *18*, 817.
(28) Todd, B. D.; Evans, D. J.; Daivis, P. J. *Phys. Rev. E* **1995**, *52*, 1627.
(29) Ikeshoji, T.; Hafskjold, B.; Furuholt, H. *Mol. Simul.* **2003**, *29*, 101.
(30) Todd, B. D.; Evans, D. J. *J. Chem. Phys.* **1995**, *103*, 9804.
(31) Røsjorde, A.; Fossmo, D. W.; Bedeaux, D.; Kjelstrup S.; Hafskjold, B. *J. Colloid Interface Sci.* **2000**, *232*, 1.
(32) Johannessen, E.; Bedeaux, D. *Physica A* **2003**, *330*, 354.
(33) Nagayama, G.; Tsuruta, T. *J. Chem. Phys.* **2003**, *118*, 1392.
(34) Bedeaux, D.; Kjelstrup, S.; Rubi, M. *J. Chem. Phys.* **2003**, *119*, 9163.
(35) Kjelstrup, S.; Tsuruta, T.; Bedeaux, D. *J. Colloid Interface Sci.* **2002**, *256*, 451.
(36) Olivier, M.-L.; Rollier, J.-D.; Kjelstrup, S. *Colloids Surf. A: Physicochem. Eng. Aspects* **2002**, *210*, 199.